

Article

Surface Plasmon Polariton Triggered Generation of 1D-Low Spatial Frequency LIPSS on Fused Silica

Simon Schwarz ^{1,*}, Stefan Rung ¹, Cemal Esen ² and Ralf Hellmann ¹

¹ Applied Laser and Photonics Group, University of Applied Sciences Aschaffenburg, Würzburger Straße 45, 63743 Aschaffenburg, Germany; stefan.rung@h-ab.de (S.R.); ralf.hellmann@h-ab.de (R.H.)

² Applied Laser Technologies, Ruhr-Universität Bochum, Universitätsstraße 150, 44801 Bochum, Germany; esen@lat.rub.de

* Correspondence: simon.schwarz@h-ab.de; Tel.: +49-6022-81-3644

Received: 13 August 2018; Accepted: 9 September 2018; Published: 12 September 2018



Abstract: We report on the generation of low spatial frequency laser-induced periodic surface structures along straight lines on fused silica by spatially scanning the laser parallel to its polarization direction. The influence of the applied laser fluence and the scanning speed on the periodic surface structures is investigated. The parameter study shows that periodic structures appear in a limited parameter regime of combined fluence and scan speed with periodicities smaller than the laser wavelength. Most strikingly, we observe a perpendicular orientation of the self-assembled periodic structures to the electrical field of the laser, notably a previously unreported result for this dielectric material. This behavior is explained taking into account calculations of surface plasmon polaritons including a Drude model for free carrier excitation within silica by femtosecond laser irradiation.

Keywords: laser-induced periodic surface structures; LIPSS; LSFL; surface plasmon polariton; fused silica

1. Introduction

Over the last few decades, Laser-Induced Periodic Surface Structures (LIPSS) have gained increasing attention due to the common availability of ultrashort pulsed laser sources. Additionally, intensified research has been raised by their widely diversified potential applications in wettability [1–3], tribology [4–6], cell cultivation [7–9] or anti-reflection coating [10]. These self-assembled structures were firstly reported by Birnbaum in 1965 after irradiation of a semiconductor with a polarized laser [11]. They typically arise on solid materials upon polarized laser irradiation with the fluence being near the materials' ablation threshold [1,12,13]. LIPSS have been shown on all material classes such as conductors [1,2,14], semiconductors [5,11,12] and dielectrics [12,15,16]. Please note, due to the availability of free charge carriers, texturing conductors and semiconductors with LIPSS is significantly simpler than structuring dielectrics.

Two types of LIPSS are generally distinguished in the literature by the relation between the applied laser wavelength λ and their spatial periodicity Λ , namely Low Spatial Frequency LIPSS (LSFL) and High Spatial Frequency LIPSS (HSFL). While LSFL reveal a periodicity close to λ , HSFL have a periodicity significantly smaller than λ [12,15,17]. The origin of LSFL is described by Emmony et al. [18] as the interaction of the electromagnetic field of the laser and a surface scattered wave generated by the incident laser light. This surface scattered wave that forms the basis of the so-called efficacy factor theory was later associated with Surface Plasmon Polaritons (SPP) [19]. The generation of surface plasmon polaritons is used in several publications with respect to a better LIPSS understanding [17,20–23]. SPP are formed, e.g., on a metal-dielectric interface with ambient

air acting like a dielectric with positive permittivity ($\epsilon > 0$) and metals having a negative permittivity ($\epsilon < 0$) [21,22,24,25]. For the generation of LSFL on a dielectric material such as glass in ambient air with positive permittivity, however, the conditions for SPP excitation are not fulfilled. Yet, for these materials, LIPSS can also be generated due to the excitation of free charge carriers in the dielectric material by ultrashort pulsed laser irradiation, turning the dielectric surface into a metallic state [17,20–22]. This excitation mechanism is related to multiphoton and avalanche ionization processes [26].

While the majority of scientific studies of LSFL on dielectric materials are based on punctual structures [12,15,27,28], i.e., LSFL are generated on a single spot only, for industrial applications, the generation of one- and two-dimensional LSFL is mandatory by scanning the laser. For metals [1–4,14,29,30] and semiconductors [5,31–33], this has been shown in several publications because of the convenience in generating LSFL on these materials with free charged carriers ($\epsilon < 0$). For dielectric materials, e.g., fused silica, the authors recently have shown the transfer from punctual laser irradiation into the dynamic range, i.e., moving the laser spot over the sample [16]. However, these so-called one-Dimensional LSFL (1D-LSFL) reveal periodicities larger than the wavelength of the applied laser and an orientation parallel to the polarization of the laser under normal irradiation, and neither conform with the established SPP theory. This supra-wavelength ($\Lambda_{LSFL} > \lambda$) type of LIPSS has been reported in several publications for punctual laser irradiation of dielectrics [34–36] with their generation being attributed to hydrodynamic instabilities within a convection roll-driven formation [34]. Beside these supra-wavelength structures, the common way LSFL are shown on fused silica for punctual irradiation is $\Lambda_{LSFL} < \lambda$ and still being parallel to the polarization of the laser [12,15,28,36]. These parallel-oriented structures are attributed to radiation remnants [13,37].

SPP-generated LSFL having an orientation perpendicular to the polarization of the laser with $\Lambda_{LSFL} < \lambda$ on fused silica have been calculated by Höhm et al. [38] within the efficacy factor theory for excited high carrier concentrations. However, Höhm et al. never observed such oriented structures experimentally. Rudenko et al. [39] performed numerical simulations regarding the generation of both HSFL and LSFL on fused silica. Their simulations revealed the generation of LSFL being parallel to the polarization of the laser deeper in the material due to far-field interaction without a plasmonic electromagnetic scenario (low carrier densities). The transition from HSFL to these type of LSFL is executed by the removal of the material at carrier densities below or near a critical carrier concentration. Furthermore, their calculations showed that LSFL that are oriented perpendicularly are hard to generate due to the removal of the material by ablation. For the non-scanning case, we also observed these parallel LSFL in a previous study, but never found LSFL with a perpendicular orientation [28]. Xu et al. [40] found LSFL on fused silica oriented parallel to the polarization of the laser for both, scanning perpendicularly and parallel to the laser polarization. For perpendicular scanning, we also observed parallel-oriented structures in a previous publication [16]. Therefore, we assume that the scanning direction (parallel to the polarization) in combination with the ideal parameters is the key to overcome this limitation for generating LSFL with an orientation perpendicular to the laser polarization.

Against this background, in this contribution, we report on a detailed evaluation of 1D-LSFL generated with a 1030-nm femtosecond laser on fused silica. The influence of the laser fluence and the scanning speed by scanning parallel to the polarization of the laser on LSFL is investigated. To the best of our knowledge, we show an unreported phenomenon on fused silica, namely a perpendicular orientation of LSFL versus laser polarization. However, the periodicity of the structures reveals values between 0.9 μm and 1.0 μm , i.e., being smaller than the laser wavelength.

2. Experimental Section

An ultrashort pulsed laser (Pharos, Light Conversion Ltd., Vilnius, Lithuania) equipped with a micromachining system with a galvo scanner (RTA AR800 2G+, Newson, Dendermonde, Belgium) and an f- Θ -lens mounted on an adjustable z-stage were used. The f- Θ -lens having a focal length of

100 mm leads to a Gaussian beam diameter $2\omega_0$ of 31 μm ($1/e^2$), with ω_0 the beam radius in the focal plane as measured with a high-resolution CCD camera (UI-1490SE-M-GL, IDS). The ultrashort pulsed laser is specified by a wavelength of 1030 nm and a pulse width of 230 fs (FWHM) at a repetition rate of 50 kHz in our experiments. The polarization is controlled with a $\lambda/2$ -plate, while the pulse energy E_p , and thereby, the applied fluence Φ , defined to be $\Phi = E_p/(\pi\omega_0^2)$, is adjusted by an external attenuator. Natural fused silica has been chosen as a prominent candidate of a dielectric material with a large band gap. Figure 1 shows the used experimental setup, including the scanning direction and polarization of the laser, as well as the orientation of the generated structures. The structures and their surface modifications are analyzed in detail with a Scanning Electron Microscope (SEM, Phenom ProX, Phenom-World, Eindhoven, The Netherlands), an Atomic Force Microscope (AFM, Dimension Icon, Bruker, Billerica, MA, USA) and a transmitted light microscope (DM6000 M, Leica, Wetzlar, Germany). For the interpretation of the experimental results, the established method of transferring captured microscope pictures into Fourier spectra is used [12]. The geometrical dimensions of LSFL are captured via SEM with subsequent image analysis via 2D Fourier transformation. Based on Equation (1), the two-dimensional discrete Fourier transform of the SEM image can be calculated by:

$$F(u, v) = \sum_{x=0}^{X-1} \sum_{y=0}^{Y-1} f(x, y) * e^{-i2\pi \frac{xu}{X}} * e^{-i2\pi \frac{yv}{Y}} \quad (1)$$

wherein u and v are spatial frequencies in the x and y directions, respectively, and $F(u, v)$ is the two-dimensional spectrum of the microscope image $f(x, y)$. X and Y represent the size of the image $f(x, y)$.

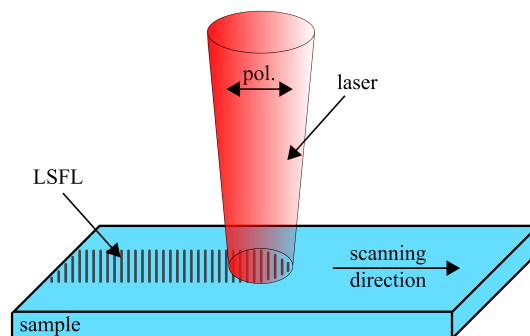
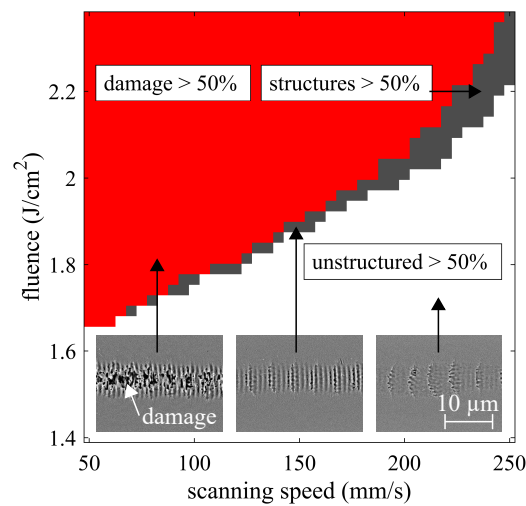


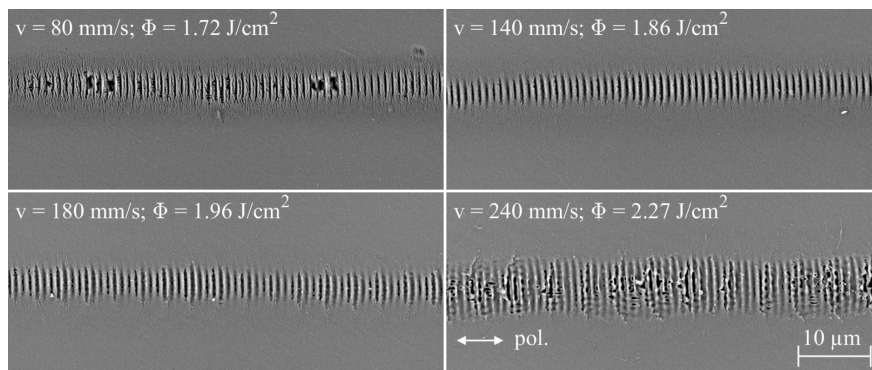
Figure 1. Schematic illustration of the experimental setup with the scanning direction being parallel to the polarization (pol.) of the laser.

3. Results and Discussion

To generate one-dimensional LSFL, the laser spot was translated across the fused silica specimen by the scanner. For the parameter study, we defined a 41×41 matrix varying the fluence between 1.40 J/cm^2 and 2.37 J/cm^2 and the laser scanning speed between 50 mm/s and 250 mm/s (i.e., 1681 parameter sets), respectively. Figure 2a summarizes the results for the generation of one-dimensional structures, where we distinguish three regions. For Region I, the scanned lines include more than 50% surface damage (damage > 50%). In Region II, the scanned lines include more than 50% periodic structures (structures > 50%), and finally, in Region III, the scanned lines include more than 50% unstructured areas (unstructured > 50%), respectively. Insets in Figure 2a show examples for the three regions. Apparently, the parameter range including lines with more than 50% periodic structures is a narrow band of combined fluence and scan speed. In addition, 1D-LSFL generation with increasing scanning speeds needs higher fluences to guarantee a certain energy input.



(a)



(b)

Figure 2. (a) A 41×41 matrix including scanning speed variations between 50 mm/s and 250 mm/s and fluence variations between 1.40 J/cm² and 2.37 J/cm²; scanning direction is set parallel to the laser polarization. Different regimes determine whether the line includes more than 50% damaged, structured and unstructured areas. (b) SEM images of 1D-LSFL on fused silica including more than 50% structures (Region II) for different scanning speeds and fluences.

Figure 2b shows SEM images of 1D-LSFL in Region II, i.e., more than 50% of the surface exhibits periodic structures, being generated with different scanning speeds and fluences. Please note that the scanning direction was set parallel to the polarization of the laser (white arrow). Obviously, the generated structures are perpendicular to the laser polarization. Contrary to these observations, different authors reported on the generation of LSFL on fused silica with an orientation being parallel to the polarization of the laser for both scanning and non-scanning (punctual) cases [12,15,16,36,40]. These parallel structures were never observed in our experiment over the entire parameter range in Figure 2a. Furthermore, the observed LSFL reveal periodicities smaller than the wavelength of the laser with the values summarized in Table 1.

Figure 3 shows an AFM image having a field of view of $10 \mu\text{m} \times 10 \mu\text{m}$ (a) and the corresponding modulation profile (b) of the shown structures. The laser parameters are the same as in Figure 2b for the qualitatively most homogeneous 1D-LSFL (140 mm/s and 1.86 J/cm²). The structures reveal an average depth of about 260 nm and a modulation profile resembling a $|\sin(x)|$ function.

Table 1. Periodicities of the one-dimensional LSFL for different fluences and scanning speeds. Periodicities are determined via transferring the SEM pictures in the Fourier spectra.

v (mm/s)	Φ (J/cm ²)	Λ _{LSFL} (nm)
80	1.72	932
100	1.77	948
120	1.79	950
140	1.86	964
160	1.91	962
180	1.96	962
200	2.03	980
220	2.10	980
240	2.27	977

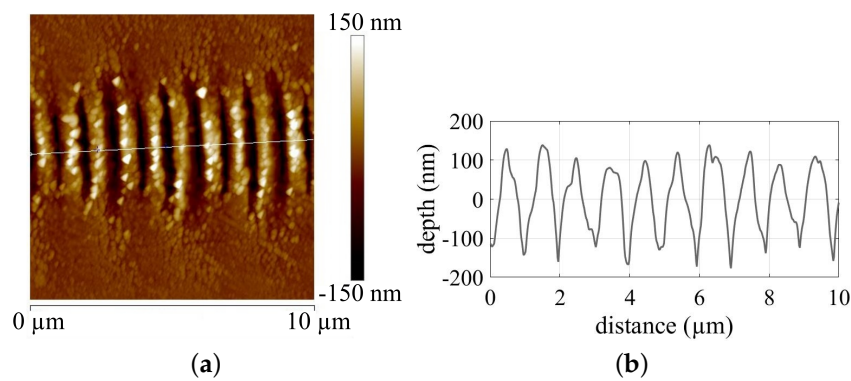


Figure 3. (a) AFM image of one-dimensional LSFL for scanning with v = 140 mm/s and Φ = 1.86 J/cm²; (b) corresponding modulation profile revealing an average depth of about 260 nm and a modulation profile resembling a |sin(x)| function.

According to the SPP theory, surface plasmon polaritons are formed at a metal-dielectric interface [21–24,41], while their periodicity is calculated with an established equation for the real part of ε_m (Equation (2)) [20–23,42]. Here, λ_{SPP} describes the wavelength of the SPP, λ₀ the wavelength of the applied laser, ε'_m the real part of the dielectric function of the metallic substrate (ε_m = ε'_m + iε''_m) and ε_d the dielectric function of the dielectric.

$$\lambda_{SPP} = \Lambda_{LSFL} = \lambda_0 * \sqrt{\frac{\epsilon'_m + \epsilon_d}{\epsilon'_m \epsilon_d}} \tag{2}$$

For laser irradiation in ambient air, the dielectric function ε_d corresponds to ε_d = 1, where the real part of ε_m has to be ε'_m < -1. For normal incidence, the LSFL periodicity Λ_{LSFL} equals λ_{SPP}, and the orientation of the LSFL is expected to be perpendicular to the polarization of the laser due to the Transverse Magnetic (TM) characteristics of the surface plasmons [20].

For dielectric materials, such as fused silica, the complex refractive index is n = 1.45 + i0 [43], and therefore, the dielectric function ε_m = n² is not fulfilling ε'_m < -1. In the case of ultrashort pulse laser irradiation, the dielectric function of the fused silica specimen is altered due to photo- and avalanche ionization [26]. These mechanisms excite electrons from the valance into the conduction band of the material. Above a certain carrier density N_e, the dielectric material turns into a transient metallic state [17,20–22], allowing the generation of SPP. The new complex dielectric function ε_m^{*} = ε_m^{*} + iε_m^{**} = ε_m + ε_{Drude} of the irradiated material is calculated with a Drude model described by Equation (3) [44]. Here, e is the electron charge, ε₀ the vacuum dielectric function, m_e the free

electron mass, $\omega = 2\pi c/\lambda$ the optical frequency, $m_{opt}^* = 0.49$ [38] the optical effective mass and $\tau_D = 0.4$ fs [38] the Drude damping time.

$$\epsilon_{Drude} = -\frac{e^2 N_e}{\epsilon_0 m_{opt}^* m_e \omega^2 (1 + \frac{i}{\omega \tau_D})} \quad (3)$$

Figure 4a shows the evolution of the complex dielectric function of fused silica for different carrier densities. While the imaginary part $\epsilon_m^{*''}$ becomes greater for increasing carrier densities, the real part $\epsilon_m^{*'}$ decreases. For a carrier density of $4.58 \times 10^{21} \text{ cm}^{-3}$, the real part becomes smaller than -1 , fulfilling $\epsilon_m^{*' < -1$ and thus enabling the generation of SPP. Figure 4b depicts the periodicity of λ_{SPP} for increasing N_e , starting at a value of $4.58 \times 10^{21} \text{ cm}^{-3}$ ($\epsilon_m^{*' < -1$). Please note, $\epsilon_m^{*'}$ in Equation (2) is replaced by the real part of ϵ_m^* for this approximation. Obviously, the periodicity of λ_{SPP} is dependent on the excited carrier density, and λ_{SPP} does not cross the critical value of 1030 nm (laser wavelength). Furthermore, the increasing LSFL periodicities for larger carrier densities are also suggested from Table 1 for increasing fluence levels. The marked area in Figure 4b shows the regime of the LSFL listed in Table 1, with $932 \text{ nm} < \Lambda_{LSFL} > 980 \text{ nm}$. The corresponding carrier densities are between $1.13 \times 10^{22} \text{ cm}^{-3}$ and $1.87 \times 10^{22} \text{ cm}^{-3}$. Again, the SPP theory describes the LSFL generation to be perpendicular to the laser polarization having a wavelength smaller than the laser wavelength, both confirmed by the periodic structures shown in Figure 1.

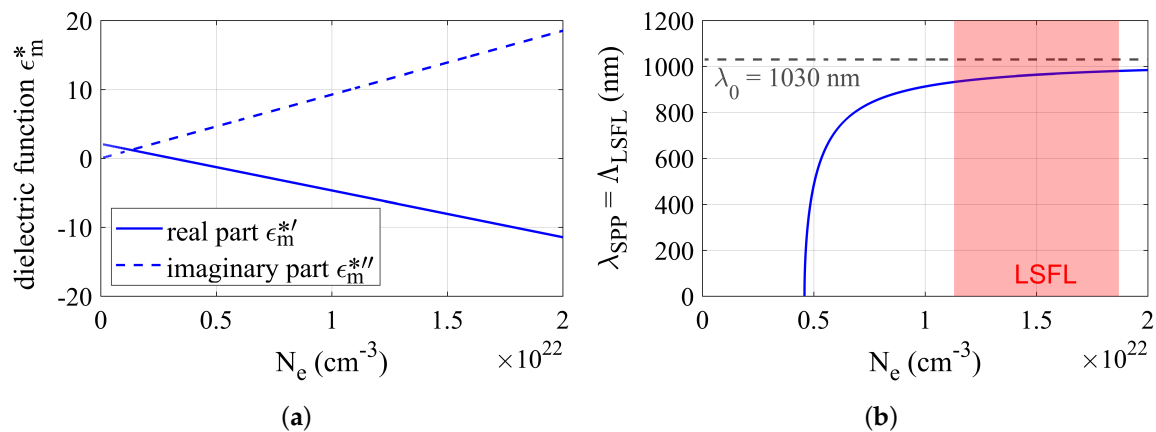


Figure 4. (a) Dielectric function (ϵ_m^*) of fused silica calculated with a Drude model for femtosecond laser irradiation; (b) periodicity of the generated surface plasmon polaritons (λ_{SPP}) for increasing carrier density N_e , the red area marking the periodicities labeled in Table 1.

4. Conclusions

We have presented experimental and numerical results on the generation of one-dimensional periodical structures on fused silica, having a special focus on the scanning direction being parallel to the laser polarization. By varying the laser fluence and scanning speed of a femtosecond laser, we identified a parameter regime that leads to a preferential LSFL generation with periodicities smaller than the laser wavelength. In addition, we observed the predicted, yet previously unreported, orientation of LSFL on fused silica being perpendicular to the electrical field of the laser. The generation of LSFL with periodicities smaller than the laser wavelength is in accordance with the calculations within SPP theory.

Author Contributions: S.S. and S.R. conceived, designed and performed the experiments and analyzed the data. S.S., C.E. and R.H. wrote the paper.

Funding: This research received no external funding.

Conflicts of Interest: The authors declare no conflict of interest.

References

1. Cunha, A.; Serro, A.P.; Oliveira, V.; Almeida, A.; Vilar, R.; Durrieu, M.C. Wetting behavior of femtosecond laser textured Ti–6Al–4V surfaces. *Appl. Surf. Sci.* **2013**, *265*, 688–696. [[CrossRef](#)]
2. Bizi-Bandoki, P.; Benayoun, S.; Valette, S.; Beaugiraud, B.; Audouard, E. Modifications of roughness and wettability properties of metals induced by femtosecond laser treatment. *Appl. Surf. Sci.* **2011**, *257*, 5213–5218. [[CrossRef](#)]
3. Jagdheesh, R.; Pathiraj, B.; Karatay, E.; Römer, G.R.B.E.; Huis in't Veld, A.J. Laser-induced nanoscale superhydrophobic structures on metal surfaces. *Langmuir ACS J. Surf. Colloids* **2011**, *27*, 8464–8469. [[CrossRef](#)] [[PubMed](#)]
4. Wang, Z.; Zhao, Q.; Wang, C. Reduction of Friction of Metals Using Laser-Induced Periodic Surface Nanostructures. *Micromachines* **2015**, *6*, 1606–1616. [[CrossRef](#)]
5. Eichstädt, J.; Römer, G.; Huis in't Veld, A.J. Towards Friction Control using laser-induced periodic Surface Structures. *Phys. Procedia* **2011**, *12*, 7–15. [[CrossRef](#)]
6. Yasumaru, N.; Miyazaki, K.; Kiuchi, J. Control of tribological properties of diamond-like carbon films with femtosecond-laser-induced nanostructuring. *Appl. Surf. Sci.* **2008**, *254*, 2364–2368. [[CrossRef](#)]
7. Rebollar, E.; Frischauf, I.; Olbrich, M.; Peterbauer, T.; Hering, S.; Preiner, J.; Hinterdorfer, P.; Romanin, C.; Heitz, J. Proliferation of aligned mammalian cells on laser-nanostructured polystyrene. *Biomaterials* **2008**, *29*, 1796–1806. [[CrossRef](#)] [[PubMed](#)]
8. Wallat, K.; Dörr, D.; Le Harzic, R.; Stracke, F.; Sauer, D.; Neumeier, M.; Kovtun, A.; Zimmermann, H.; Epple, M. Cellular reactions toward nanostructured silicon surfaces created by laser ablation. *J. Laser Appl.* **2012**, *24*, 042016. [[CrossRef](#)]
9. Wang, X.; Ohlin, C.A.; Lu, Q.; Hu, J. Cell directional migration and oriented division on three-dimensional laser-induced periodic surface structures on polystyrene. *Biomaterials* **2008**, *29*, 2049–2059. [[CrossRef](#)] [[PubMed](#)]
10. Granados, E.; Martinez-Calderon, M.; Gomez, M.; Rodriguez, A.; Olaizola, S.M. Photonic structures in diamond based on femtosecond UV laser induced periodic surface structuring (LIPSS). *Opt. Express* **2017**, *25*, 15330–15335. [[CrossRef](#)] [[PubMed](#)]
11. Birnbaum, M. Semiconductor Surface Damage Produced by Ruby Lasers. *J. Appl. Phys.* **1965**, *36*, 3688–3689. [[CrossRef](#)]
12. Bonse, J.; Krüger, J.; Höhm, S.; Rosenfeld, A. Femtosecond laser-induced periodic surface structures. *J. Laser Appl.* **2012**, *24*, 042006. [[CrossRef](#)]
13. Sipe, J.E.; Young, J.F.; Preston, J.S.; van Driel, H.M. Laser-induced periodic surface structure. I. Theory. *Phys. Rev. B* **1983**, *27*, 1141–1154. [[CrossRef](#)]
14. Preusch, F.; Rung, S.; Hellmann, R. Influence of Polishing Orientation on the Generation of LIPSS on Stainless Steel. *J. Laser Micro/Nanoeng.* **2016**, *11*, 137–142. [[CrossRef](#)]
15. Fang, Z.; Zhao, Y.; Shao, J. Femtosecond laser-induced periodic surface structure on fused silica surface. *Opt. Int. J. Light Electron Opt.* **2016**, *127*, 1171–1175. [[CrossRef](#)]
16. Schwarz, S.; Rung, S.; Hellmann, R. One-dimensional low spatial frequency LIPSS with rotating orientation on fused silica. *Appl. Surf. Sci.* **2017**, *411*, 113–116. [[CrossRef](#)]
17. Kuladeep, R.; Sahoo, C.; Narayana Rao, D. Direct writing of continuous and discontinuous sub-wavelength periodic surface structures on single-crystalline silicon using femtosecond laser. *Appl. Phys. Lett.* **2014**, *104*, 222103. [[CrossRef](#)]
18. Emmony, D.C.; Howson, R.P.; Willis, L.J. Laser mirror damage in germanium at 10.6 μm . *Appl. Phys. Lett.* **1973**, *23*, 598. [[CrossRef](#)]
19. Bonse, J.; Rosenfeld, A.; Krüger, J. On the role of surface plasmon polaritons in the formation of laser-induced periodic surface structures upon irradiation of silicon by femtosecond-laser pulses. *J. Appl. Phys.* **2009**, *106*, 104910. [[CrossRef](#)]
20. Huang, M.; Zhao, F.; Cheng, Y.; Xu, N.; Xu, Z. Origin of laser-induced near-subwavelength ripples: Interference between surface plasmons and incident laser. *ACS Nano* **2009**, *3*, 4062–4070. [[CrossRef](#)] [[PubMed](#)]

21. Nürnberger, P.; Reinhardt, H.M.; Kim, H.C.; Pfeifer, E.; Kroll, M.; Müller, S.; Yang, F.; Hampp, N.A. Orthogonally superimposed laser-induced periodic surface structures (LIPSS) upon nanosecond laser pulse irradiation of SiO₂ /Si layered systems. *Appl. Surf. Sci.* **2017**, *425*, 682–688. [[CrossRef](#)]
22. Das, S.K.; Messaoudi, H.; Debroy, A.; McGlynn, E.; Grunwald, R. Multiphoton excitation of surface plasmon-polaritons and scaling of nanoripple formation in large bandgap materials. *Opt. Mater. Express* **2013**, *3*, 1705–1715. [[CrossRef](#)]
23. Pan, A.; Dias, A.; Gomez-Aranzadi, M.; Olaizola, S.M.; Rodriguez, A. Formation of laser-induced periodic surface structures on niobium by femtosecond laser irradiation. *J. Appl. Phys.* **2014**, *115*, 173101. [[CrossRef](#)]
24. Rizal, C.; Pisana, S.; Hrvoic, I. Improved Magneto-Optic Surface Plasmon Resonance Biosensors. *Photonics* **2018**, *5*, 15. [[CrossRef](#)]
25. Rizal, C.; Pisana, S.; Hrvoic, I.; Fullerton, E.E. Microstructure and magneto-optical surface plasmon resonance of Co/Au multilayers. *J. Phys. Commun.* **2018**, *2*, 055010. [[CrossRef](#)]
26. Stuart, B.C.; Feit, M.D.; Rubenchik, A.M.; Shore, B.W.; Perry, M.D. Laser-Induced Damage in Dielectrics with Nanosecond to Subpicosecond Pulses. *Phys. Rev. Lett.* **1995**, *74*, 2248–2251. [[CrossRef](#)] [[PubMed](#)]
27. Jiang, L.; Shi, X.; Li, X.; Yuan, Y.; Wang, C.; Lu, Y. Subwavelength ripples adjustment based on electron dynamics control by using shaped ultrafast laser pulse trains. *Opt. Express* **2012**, *20*, 21505–21511. [[CrossRef](#)] [[PubMed](#)]
28. Schwarz, S.; Rung, S.; Hellmann, R. Generation of laser-induced periodic surface structures on transparent material-fused silica. *Appl. Phys. Lett.* **2016**, *108*, 181607. [[CrossRef](#)] Corrected in: Erratum: “Generation of laser-induced periodic surface structures on transparent material-fused silica”. *Appl. Phys. Lett.* **2018**, *113*, 049901. [[CrossRef](#)]
29. Gnilitzky, I.; Derrien, T.J.Y.; Levy, Y.; Bulgakova, N.M.; Mocek, T.; Orazi, L. High-speed manufacturing of highly regular femtosecond laser-induced periodic surface structures: Physical origin of regularity. *Sci. Rep.* **2017**, *7*, 8485. [[CrossRef](#)] [[PubMed](#)]
30. Ruiz de la Cruz, A.; Lahoz, R.; Siegel, J.; de la Fuente, G.F.; Solis, J. High speed inscription of uniform, large-area laser-induced periodic surface structures in Cr films using a high repetition rate fs laser. *Opt. Lett.* **2014**, *39*, 2491–2494. [[CrossRef](#)] [[PubMed](#)]
31. Hong, L.; Wang, X.C.; Zheng, H.Y.; Wang, H.; Yu, H.Y. Femtosecond laser fabrication of large-area periodic surface ripple structure on Si substrate. *Appl. Surf. Sci.* **2014**, *297*, 134–138. [[CrossRef](#)]
32. Fuentes-Edfuf, Y.; Garcia-Lechuga, M.; Puerto, D.; Florian, C.; Garcia-Leis, A.; Sanchez-Cortes, S.; Solis, J.; Siegel, J. Coherent scatter-controlled phase-change grating structures in silicon using femtosecond laser pulses. *Sci. Rep.* **2017**, *7*, 4594. [[CrossRef](#)] [[PubMed](#)]
33. Das, S.K.; Dasari, K.; Rosenfeld, A.; Grunwald, R. Extended-area nanostructuring of TiO₂ with femtosecond laser pulses at 400 nm using a line focus. *Nanotechnology* **2010**, *21*, 155302. [[CrossRef](#)] [[PubMed](#)]
34. Tsibidis, G.D.; Skoulas, E.; Papadopoulos, A.; Stratakis, E. Convection roll-driven generation of supra-wavelength periodic surface structures on dielectrics upon irradiation with femtosecond pulsed lasers. *Phys. Rev. B* **2016**, *94*, 081305. [[CrossRef](#)]
35. Seifert, G.; Kaempfe, M.; Syrowatka, F.; Harnagea, C.; Hesse, D.; Graener, H. Self-organized structure formation on the bottom of femtosecond laser ablation craters in glass. *Appl. Phys. A* **2005**, *81*, 799–803. [[CrossRef](#)]
36. Gräf, S.; Kunz, C.; Müller, F.A. Formation and Properties of Laser-Induced Periodic Surface Structures on Different Glasses. *Materials* **2017**, *10*. [[CrossRef](#)] [[PubMed](#)]
37. Bonse, J.; Hohm, S.; Kirner, S.V.; Rosenfeld, A.; Kruger, J. Laser-Induced Periodic Surface Structures—A Scientific Evergreen. *IEEE J. Sel. Top. Quantum Electron.* **2017**, *23*, 1–15. [[CrossRef](#)]
38. Höhm, S.; Rosenfeld, A.; Krüger, J.; Bonse, J. Femtosecond laser-induced periodic surface structures on silica. *J. Appl. Phys.* **2012**, *112*, 014901. [[CrossRef](#)]
39. Rudenko, A.; Colombier, J.P.; Höhm, S.; Rosenfeld, A.; Krüger, J.; Bonse, J.; Itina, T.E. Spontaneous periodic ordering on the surface and in the bulk of dielectrics irradiated by ultrafast laser: A shared electromagnetic origin. *Sci. Rep.* **2017**, *7*, 12306. [[CrossRef](#)] [[PubMed](#)]
40. Xu, S.Z.; Dou, H.Q.; Sun, K.; Ye, Y.Y.; Li, Z.; Wang, H.J.; Liao, W.; Liu, H.; Miao, X.X.; Yuan, X.D.; et al. Scan speed and fluence effects in femtosecond laser induced micro/nano-structures on the surface of fused silica. *J. Non-Cryst. Solids* **2018**, *492*, 56–62. [[CrossRef](#)]

41. Rizal, C.; Moa, B.; Niraula, B.B. Ferromagnetic Multilayers: Magnetoresistance, Magnetic Anisotropy, and Beyond. *Magnetochemistry* **2016**, *2*. [[CrossRef](#)]
42. Garrelie, F.; Colombier, J.P.; Pigeon, F.; Tonchev, S.; Faure, N.; Bounhalli, M.; Reynaud, S.; Parriaux, O. Evidence of surface plasmon resonance in ultrafast laser-induced ripples. *Opt. Express* **2011**, *19*, 9035–9043. [[CrossRef](#)] [[PubMed](#)]
43. Malitson, I.H. Interspecimen Comparison of the Refractive Index of Fused Silica. *J. Opt. Soc. Am.* **1965**, *55*, 1205. [[CrossRef](#)]
44. Dufft, D.; Rosenfeld, A.; Das, S.K.; Grunwald, R.; Bonse, J. Femtosecond laser-induced periodic surface structures revisited: A comparative study on ZnO. *J. Appl. Phys.* **2009**, *105*, 034908. [[CrossRef](#)]



© 2018 by the authors. Licensee MDPI, Basel, Switzerland. This article is an open access article distributed under the terms and conditions of the Creative Commons Attribution (CC BY) license (<http://creativecommons.org/licenses/by/4.0/>).